Neuron, Vol. 43, 883–896, September 16, 2004, Copyright ©2004 by Cell Press

Oscillatory Entrainment of Striatal Neurons in Freely Moving Rats

Joshua D. Berke,[1,*] Murat Okatan, Jennifer Skurski, and Howard B. Eichenbaum
Laboratory of Cognitive Neurobiology
Boston University
Boston, Massachusetts 02215

Summary

Oscillations and synchrony in basal ganglia circuits may play a key role in the organization of voluntary actions and habits. We recorded single units and local field potentials from multiple striatal and cortical locations simultaneously, over a range of behavioral states. We observed opposite gradients of oscillatory entrainment, with dorsal/lateral striatal neurons entrained to high-voltage spindle oscillations ("spike wave discharges") and ventral/medial striatal neurons entrained to the hippocampal theta rhythm. While the majority of units were likely medium-spiny projection neurons, a second neuronal population showed characteristic features of fast-spiking GABAergic interneurons, including tonic activity, brief waveforms, and high-frequency bursts. These fired at an earlier spindle phase than the main neuronal population, and their density within striatum corresponded closely to the intensity of spindle oscillations. The orchestration of oscillatory activity by networks of striatal interneurons may be an important mechanism in the pathophysiology of neurological disorders such as Parkinson's disease.

Introduction

Neuronal pathways from the cerebral cortex through the basal ganglia, to thalamus, and back to cortex are critical for the normal selection and initiation of actions (Graybiel et al., 1994) and for the learning of habits and skills (White, 1997; Eichenbaum and Cohen, 2001). Abnormal function of these circuits is thought to underlie a host of human neurological and psychiatric disorders, including Parkinson's disease, obsessive-compulsive disorder, and drug addiction (Albin et al., 1989; Cummings, 1993; Berke and Hyman, 2000). Oscillations in cortex-basal ganglia networks have been argued to be crucial to their normal and altered function (Brown and Marsden, 1998) and have been investigated in slice cultures (Plenz and Kitai, 1999), anesthetized rats (Magill et al., 2000; Mahon et al., 2001), and parkinsonian humans and other primates (Bergman et al., 1998; Hurtado et al., 1999). Still, we have relatively little understanding of how patterns of neural activity are transmitted and transformed by these circuits during normal behavior.

Two prominent types of oscillation commonly observed in the EEG of awake rats are high-voltage spindles (HVSs) and the hippocampal theta rhythm. Although both are of similar frequency in awake rats (~8 Hz), they have very different distributions and behavioral correlates. High-voltage spindles (also called spike wave discharges, or mu rhythm) recruit wide regions of frontal and somatosensory cortex (Shaw, 2004). They occur only in immobile animals and disappear immediately when body movements are initiated. By contrast, the theta rhythm is strongest in moving rats, as they run through or explore an environment. Though especially prominent in the hippocampus, theta is also found in related areas such as entorhinal cortex and amygdala (Alonso and Garcia-Austt, 1987; Paré and Gaudreau, 1996). Both types of rhythm reflect the coordinated activity of large populations of individual neurons (Buzsáki, 2002; Kandel and Buzsáki, 1997), although within a brain area specific neuronal subpopulations can show distinct phase relationships (Klausberger et al., 2003).

The striatum is the largest nucleus of the basal ganglia, and it receives a wide range of neocortical, thalamic, and hippocampal inputs. Using chronically implanted microelectrodes in freely moving rats, we examined both single-unit and population activity in many striatal locations during naturally occurring sleep and wake states and behavioral task performance. We found that oscillatory activity within striatal circuits reflects the topography of striatal information processing. Within sensorimotor (dorsal/lateral) regions of striatum, neurons show strong entrainment to high-voltage spindle oscillations in the local field potential (LFP). These striatal spindle oscillations show a graded intensity distribution that closely matches the distribution of fast-spiking presumed interneurons. Burst firing of electrically coupled fast-spiking units during spindles may be important for the synchronous recruitment of medium-spiny projection units throughout sensorimotor striatum. Within more cognitive/limbic (ventral/medial) areas of the striatum, presumed spiny neurons are instead entrained to the hippocampal theta rhythm, and field potentials are coherent with hippocampal theta.

In addition to providing a framework for the classification of extracellularly recorded striatal neurons, our results shed light on the dynamic organization of cortex-basal ganglia circuits in normal, awake animals and suggest that intrastriatal interactions may be important in the spatiotemporal patterning of oscillatory activity in the basal ganglia.

Results

Distinct Classes of Striatal Neurons

We investigated the properties of striatal single units during natural sleep and wake states and during performance of a behavioral (maze) task. The great majority (340/362, 93.9%) fell into one of two distinct cell types (Figure 1). "M units" (273/362, 75.4%) had long-duration waveforms and generally low firing rates, with extended periods of silence interrupted by occasional active episodes. This firing pattern is typical of the medium-spiny

*Correspondence: jdberke@umich.edu
[1]Present address: Department of Psychology, University of Michigan, Ann Arbor, 525 East University, Ann Arbor, Michigan 48109-1109.

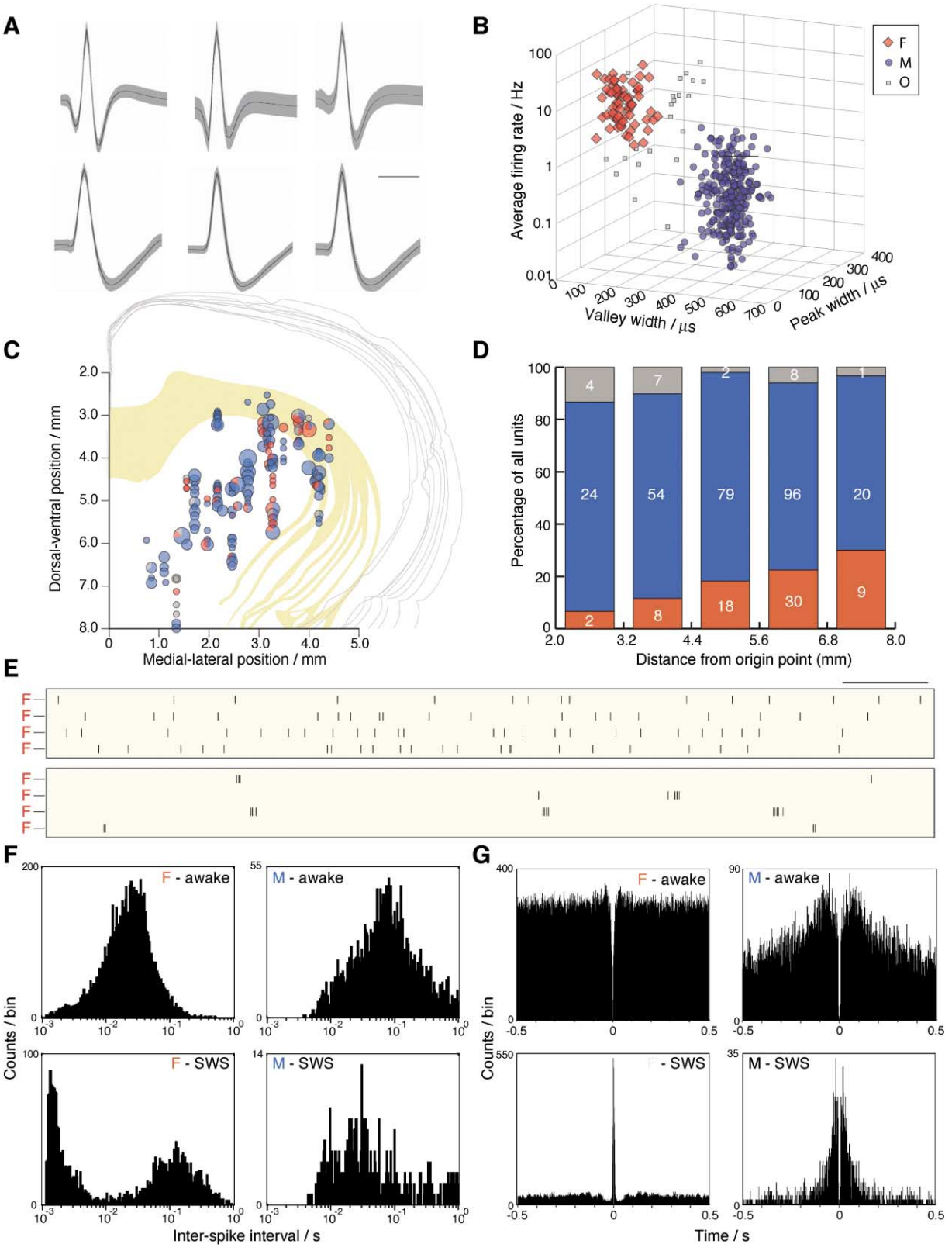

Figure 1. Properties and Distribution of Two Striatal Neuron Classes

(A) Examples of the two most common waveform types for extracellularly recorded rat striatal neurons (mean ± SD, shaded; the six waveforms are from five different rats). (Top) Brief waveforms characteristic of most tonically active units. (Bottom) Longer duration, asymmetrical waveforms characteristic of the overall majority of striatal units. Scale bar, 500 μs. Negative polarity is upward for this figure only.

projection neurons that constitute around 90%–95% of rat striatal neurons (Gerfen and Wilson, 1996). The other frequently encountered cell type, "F units" (67/362, 18.5%), was tonically active with waveforms that were very brief and usually more symmetrical. F units were not found uniformly throughout striatum but rather were common in lateral and dorsal subregions and near-absent in ventral and medial subregions (Figures 1C and 1D). This distribution is also characteristic of the fast-spiking, parvalbumin-staining GABAergic interneurons in striatum (Gerfen et al., 1985; Kita et al., 1990; Kubota et al., 1993) but not of other major types of striatal interneurons (such as those containing acetylcholine or somatostatin; Gerfen and Wilson, 1996). In awake, active animals, the tonic activity of F units came as individual spikes, but during drowsiness and slow-wave sleep, these cells switched to irregular, high-frequency bursts (Figures 1E–1G). Striatal fast-spiking GABAergic interneurons are also known to have the capacity to fire at very high frequencies (Koos and Tepper, 1999) and to have very short-duration waveforms (Kawaguchi, 1993; Plenz and Kitai, 1998). We therefore propose that our F units are the fast-spiking, parvalbumin-containing GABAergic interneurons.

Oscillatory Entrainment of Striatal Units to High-Voltage Spindles

Prominent high-voltage spindle oscillations were often observed in striatal local field potentials (Figure 2; see also Buzsáki et al., 1990; Vergnes et al., 1990). During HVSs, F units fired in a highly rhythmic manner, with bursts of activity time-locked to each cycle of the spindle (Figure 2A). Most M units analyzed (67/83, 80.1%) also showed HVS-entrained activity, though this took the form of single spikes that did not occur on every cycle. M units fired at a later phase than F units (Figures 2B and 2C). The average spike of the entrained F unit population arrived 10.0 ms before the sharp HVS peaks in the striatal LFP, while the average spike of the entrained M unit population arrived 13.0 ms after the HVS peaks. While M units in dorsal/lateral (sensorimotor) striatum were consistently HVS entrained, M units in ventral/medial (cognitive/limbic) striatum were often not HVS entrained (Figures 2D and 2E).

Graded Intensity of Striatal High-Voltage Spindles Matches the Distribution of Fast-Spiking Units

This graded distribution of cellular entrainment to HVSs was matched by a graded intensity of HVSs in the striatal LFP (Figure 3). HVSs had high power in dorsal/lateral striatum, where we found many F units and HVS-entrained M units. Conversely, HVSs were weak or absent in ventral/medial striatum, where F units were rare and M units were less likely to be HVS entrained. The gradient of spindle intensity closely matched the graded distribution of F units (Supplemental Figure S1 [http://www.neuron.org/cgi/content/full/43/6/883/DC1]; angle between gradient vectors = 5.4°). HVS cycles also differed in shape between striatal subregions. Dorsal/lateral striatal LFPs had a clear negative deflection shortly before the HVS peak (Figure 3E). This negative deflection occurs at the same time as the burst firing of the F unit population (Figures 2B and 2C); combined intracellular-extracellular recordings in striatum have previously found unit depolarization to be accompanied by negative deflections in the adjacent extracellular LFP (Leung and Yim, 1993). In more ventral-medial striatal areas, with few F units, this early negative deflection was far less apparent. In addition, HVS peaks in ventral/medial striatum lagged very slightly behind HVS peaks in dorsal/lateral striatum (Figure 3E). Taken together, this is strong evidence that HVSs in striatal LFPs reflect local cellular and/or synaptic activity rather than volume-conduction from overlying cortex.

Onset of High-Voltage Spindles Is Synchronized across Widely Separated Striatal Subregions

Striatal fast-spiking GABAergic interneurons receive direct cortical inputs and are highly sensitive to cortical activity (Parthasarathy and Graybiel, 1997). They are

(B) 3D scatter plot of cellular characteristics for 362 striatal neurons from nine rats, recorded during rest periods. Peak width at half-maximum and valley width at half-maximum were measured from the average waveform of each unit. Two major clusters were identified. "M" units (in blue) had average firing rates less than 5 Hz (mean, 0.63 ± 0.05 SEM) and valley widths greater than 300 μs (mean, 463 ± 3 SEM). "F" units (in red) had average firing rates greater than 2 Hz (mean, 15.2 ± 1.4 SEM), valley widths less than 265 μs (mean, 152 ± 5 SEM), and peak widths less than 120 μs. Other units ("O") are indicated in gray.

(C) Anatomical distribution of the striatal units described in (B) and (D). Unit positions are shown projected onto stacked coronal atlas sections from Swanson (1992), with gray lines indicating the outline of cortex and corpus callosum shown in yellow. The area of each circle is proportional to the number of units simultaneously recorded from that location; blue circle segments represent M units, red segments represent F units, gray segments represent others.

(D) Graded distribution of F units within striatum. For each unit, we measured the radial distance between its histologically reconstructed location and an origin point defined on the midline near the anterior-ventral tip of the nucleus accumbens (AP 3.13 mm anterior, ML 0, DV 8 mm below bregma; this corresponds to the axis intersection in [C]). The proportion of F units increases with increasing distance from this origin (see also Supplemental Figure S1 [http://www.neuron.org/cgi/content/full/43/6/883/DC1]) (red, F units; blue, M units; gray, others). The numbers on the bars indicate raw numbers of units in each category.

(E) State-dependent firing pattern of striatal F units. One second duration plots of spike times for four F units simultaneously recorded from a single tetrode placed in dorsal-lateral striatum. F units fire mostly single spikes when the animal is awake (top) but high-frequency bursts during slow-wave sleep ("SWS," bottom). Note that these SWS bursts are not synchronized between F units. Scale bar, 0.1 s.

(F) Log-scale interspike interval (ISI) histograms for representative individual F and M units, while animal was awake (top) or during slow-wave sleep (bottom). The two peaks seen for the F unit during SWS represent intraburst and interburst spike intervals, respectively. This pattern of high-frequency bursting during SWS (which was never observed for M units) resembles observations of some striatal fast-spiking units in slice cultures (Plenz and Aertsen, 1996; Figure 16C), although our typical intraburst ISIs of ~2 ms were shorter than their observed average value of ~9 ms.

(G) Corresponding autocorrelograms (1 ms bins) for the same F and M units as in (F). Rhythmic activity is not typically apparent during either wakefulness or SWS.

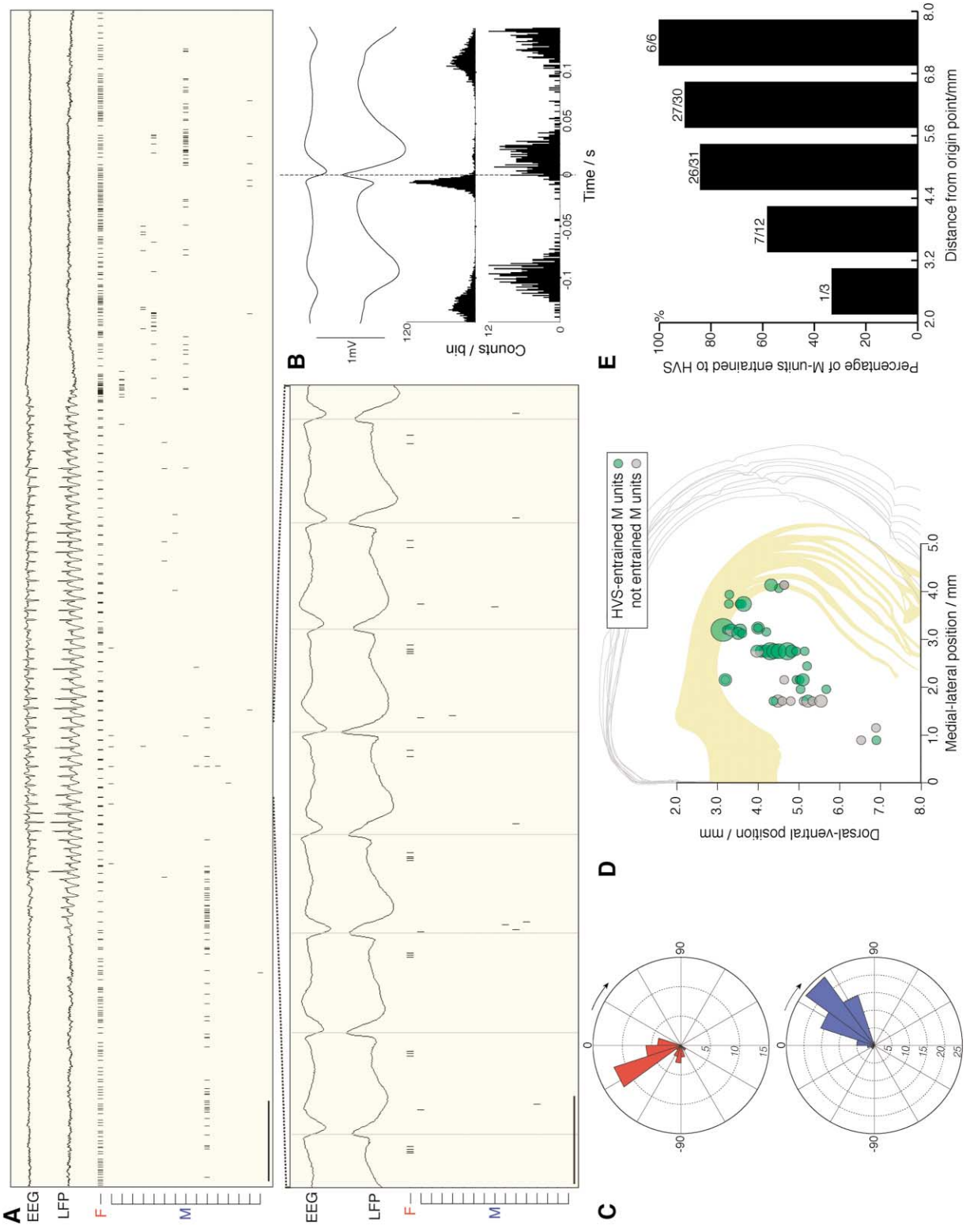

Figure 2. Striatal Unit Entrainment during High-Voltage Spindles

(A) Example of striatal single-unit entrainment during a typical high-voltage spindle event. (Upper panel) Scale bar, 1 s. (Lower panel) Scale bar, 0.1 s. The EEG shown was recorded from a skull screw over left frontal cortex (AP +4.2 mm, ML 3.5 mm relative to bregma), striatal LFP and F unit were recorded from left dorsolateral striatum (electrode #1 in Figure 3A), and 15 M units were simultaneously recorded from other striatal tetrodes. Positive polarity is upward here and in subsequent figures. F unit is strongly rhythmic during HVS events, firing on each cycle shortly before the sharp peaks in the LFP (indicated by gray bars in lower panel). The phase of this F unit is −75.6° relative to LFP peaks. During HVSs, M units generally fire single spikes, only on some cycles, and shortly after the LFP spikes.

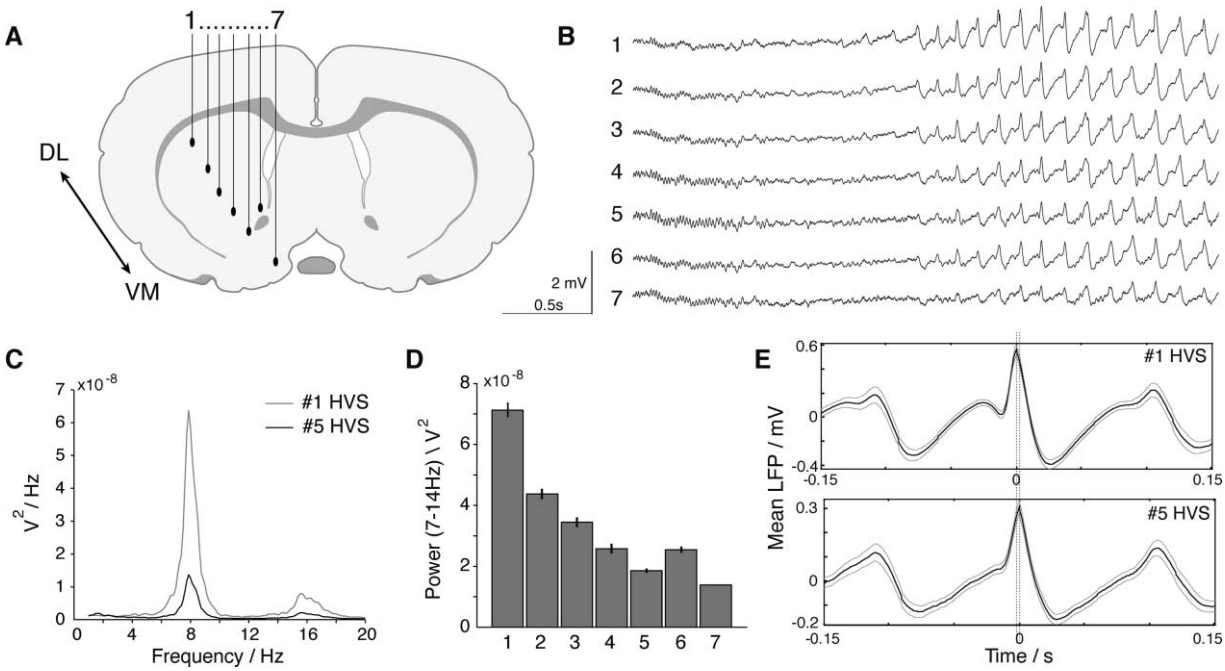

Figure 3. Graded Intensity of Striatal High-Voltage Spindle Oscillations

(A) Locations of seven tetrodes simultaneously placed along the dorsolateral-ventromedial axis of a single rat striatum (AP +0.95 mm anterior to bregma).

(B) Example of a high-voltage spindle in the LFPs recorded from the seven tetrodes illustrated in (A). High-voltage spindles are prominent in dorsal/lateral striatum and fainter in ventral/medial striatum.

(C) Power spectral density plot for the LFPs from tetrodes #1 (dorsal-lateral striatum) and #5 (nucleus accumbens) during HVS (data are from 38 detected spontaneous HVS intervals, total duration 215.6 s, over the course of a single 1978 s rest session). Peak spindle power for this animal and for others was at ~8 Hz.

(D) HVS power for each electrode depicted in (A). Bars indicate mean (± SEM) power during detected HVS intervals (see Experimental Procedures).

(E) Averaged shape of HVS cycles recorded from tetrodes #1 and #5. Each LFP was averaged around their own HVS peaks (indicated by dashed lines). However, peaks from #5 lagged behind peaks from #1 by an average of 2.38 ms (a phase difference of 6.8°). Note distinct shape of HVS cycles recorded from the two locations; in dorsal/lateral striatum there is a distinct negative deflection shortly before the mean HVS peak.

also known to be electrically coupled to each other by gap junctions on their dendrites (Kita et al., 1990; Koos and Tepper, 1999), forming a meshwork within striatum with the potential to rapidly propagate voltage changes (Gerfen and Wilson, 1996). The network of fast-spiking GABAergic interneurons may thus coordinate synchronous activity in large populations of striatal projection neurons (e.g., Koos and Tepper, 1999; Ramanathan et al., 2002), a role analogous to that played by fast-spiking interneurons in other brain regions (Cobb et al., 1995; Gibson et al., 1999; McBain and Fisahn, 2001; Galarreta and Hestrin, 2001).

If F units are indeed parvalbumin-containing GABAergic interneurons, one might therefore expect that the reliable burst firing of coupled F units during HVS epochs would cause these oscillations to be rapidly synchronized across the striatum. We found that, indeed, HVS onsets are highly synchronized between widely sepa-

(B) Relative timing of striatal LFP and action potentials during high-voltage spindles (same rat as in [A]). The top two traces show average EEG, striatal LFP in the vicinity of HVS peaks in the striatal LFP. Below this are shown corresponding cross-correlograms for individual representative F and M units (M at bottom), also oriented around the LFP peaks (dashed vertical line).

(C) Angular histograms (18° bins) indicating mean phase for all F units (top, red) and all M units (bottom, blue), relative to the sharp peaks of high-voltage spindles (at 0°). Only striatal units with a significant phase relationship ($p < 0.01$, nonparametric Rayleigh test) to spindles are included (31/35 F units and 67/83 M units tested). Other M units for which we recorded very few spikes (<20) during HVS—due to either low firing rate and/or few HVS cycles during the recording session—were excluded from analysis. Units recorded from seven rats contributed to (C)–(E) (for two other rats, HVSs were very rare or absent). The overall phase of the F unit population (−30.9°, 99% confidence limits −55.8° to −12.0°) was significantly earlier than the phase of the M unit population (41.0°, 99% confidence limits 32.6° to 48.5°).

(D) Anatomical distribution of HVS-entrained M units within striatum. Unit locations are shown mapped onto stacked coronal atlas sections as in Figure 1C. Green circles represent M units that showed a significant phase relationship to spindle peaks ($p < 0.01$ as above), while M units that were active during HVSs but not significantly entrained are shown in gray. The area of the circle is proportional to the number of units simultaneously recorded from that location.

(E) Graded distribution of HVS-entrained M units. Graph origin, bins are the same as for Figure 1D. Virtually all M units in dorsal/lateral striatum that were active during HVS were significantly ($p < 0.01$) HVS entrained.

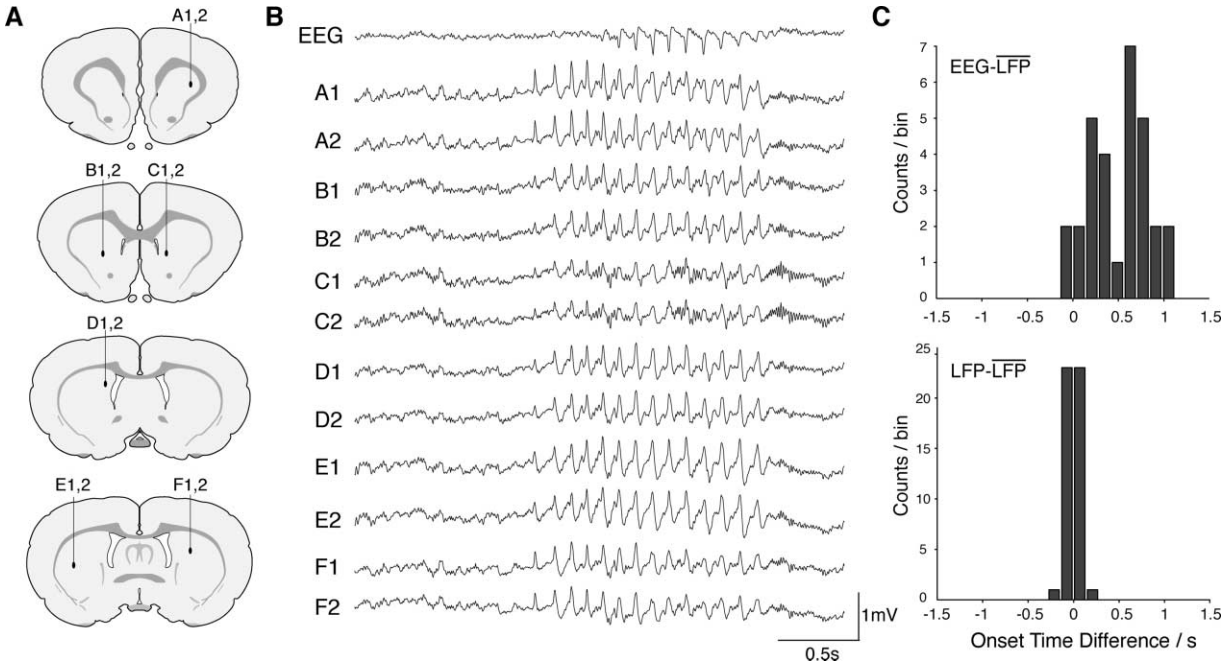

Figure 4. Widespread, Rapid Synchrony of Striatal High-Voltage Spindles

(A) Simultaneous recording from six striatal subregions ("A"–"F") from a single rat. For each site, local field potentials were recorded from each of two electrode wires ("1" and "2").

(B) Representative example of a high-voltage spindle showing early onset and high synchrony across diverse parts of striatum. EEG was recorded from a screw placed in the skull in contact with dura overlying left sensorimotor cortex (AP 3.5 mm posterior to bregma, 1.5 mm left of midline). All channels used the same reference (another screw placed in posterior lateral skull ridge).

(C) Comparison of onset times in EEG and striatal LFP (same animal as in [A] and [B]; 30 HVSs included in analysis). (Top) EEG HVS onset usually lagged mean onset time in the six striatal locations (A1, B1, C1, D1, E1, and F1 used for analysis) by a variable number of cycles. Average EEG onset lag is significantly larger than zero (0.498 s, 95% confidence limits 0.232 s, 0.763 s, by Chebyshev's inequality). (Bottom) HVS onsets were more nearly synchronous across the six striatal locations (maximum observed lag was 0.153 s after mean).

rated striatal subregions (Figure 4). By contrast, studies recording EEG from many cortical locations simultaneously have found that HVS onsets show substantial, variable lags between distinct regions of cortex, often of several cycles or more (Shaw, 2004). In our recordings, the onset of HVSs in striatal LFPs often preceded the appearance of HVSs in cortical EEG traces by as much as a second (Figures 4B and 4C). Although we did not simultaneously record from striatum and all possible cortical locations, striatal spindles were never observed to significantly lag cortical spindles. In addition, we found that HVS oscillations often occurred simultaneously across wide regions of striatum without appearing in specific cortical EEG traces (data not shown); the converse was never observed. Thus, while it remains most likely that these oscillations are initiated by cortical and thalamic circuitry, once started, HVSs become rapidly and reliably generalized across striatal regions.

Ventral/Medial Striatal Oscillations during Behavioral Task Performance

While high-voltage spindles occur in immobile animals, we also examined oscillatory entrainment of striatal neurons during active behavior. In a radial maze task, thirsty rats ran between cued goal locations where they received water rewards. During well-practiced task performance, power spectral density analysis of striatal LFPs revealed prominent peaks of oscillatory activity at theta ($\sim$8 Hz), beta ($\sim$20 Hz), and gamma ($\sim$50 Hz) frequencies (Figure 5). Each of these showed a graded distribution in striatum, being more prominent in ventral/medial striatum than in dorsal/lateral striatum. Detailed analysis of gamma power distribution (Supplemental Figure S1 [http://www.neuron.org/cgi/content/full/43/6/883/DC1]) showed that the gradient of gamma power was near-opposite to the gradient of HVS power (angle between gradient vectors = 174.5°). The different functions of dorsal/lateral (sensorimotor) striatum and ventral/medial (cognitive/limbic) striatum are thus reflected in the distinct forms of oscillatory activity found in these regions.

Relationship between Striatal and Hippocampal Theta Activity

Ventral/medial striatum receives direct inputs from the hippocampal formation, which have been proposed to have a key role in controlling the activity state of medium-spiny neurons (O'Donnell and Grace, 1995; Goto and O'Donnell, 2001b). We therefore examined the relationship between hippocampal and striatal activity in rats during performance of our radial maze task. The theta rhythm in ventral/medial striatal LFP was coherent with theta recorded from hippocampal CA1 region (Figure 5C). This coherence was reflected in the activity of individual striatal units (Figure 6). Spikes recorded from most M units in ventral/medial striatum occurred non-

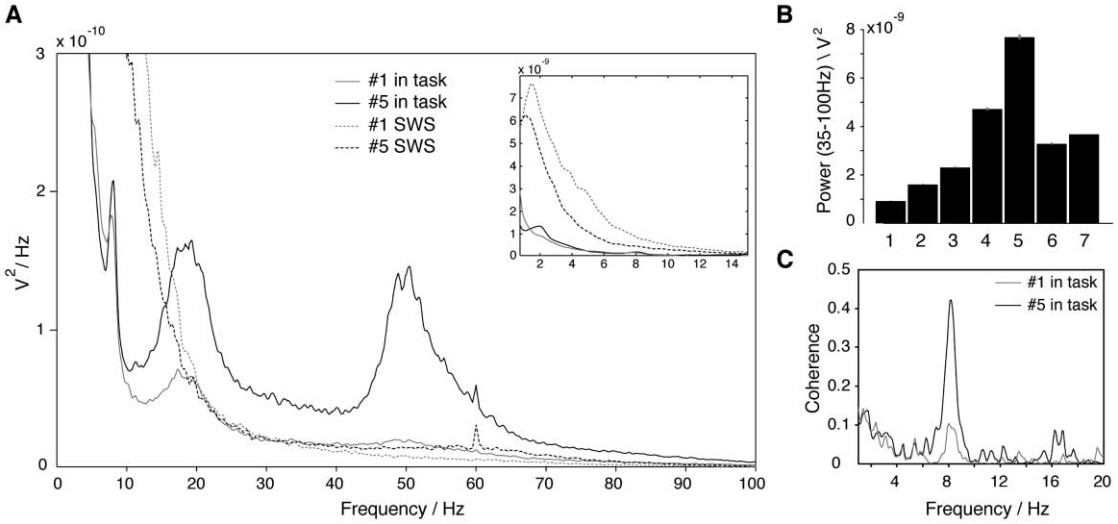

Figure 5. Oscillatory Activity in Ventral/Medial Striatum during Active Behavior

(A) LFP power spectral density plots for two striatal tetrodes (same #1 and #5 as in Figure 3A) during either epochs of slow-wave sleep during a rest session ("SWS," dashed lines; 514 s total duration) or performance of a radial maze task (solid lines; 1344 s duration). Inset shows same data on different scale for clarity. During SWS, low frequencies (slow waves) predominate in striatum just as in cortex. During task performance, three distinct peaks appear in the ventral/medial striatal LFP at theta (~8 Hz), beta (~20 Hz), and gamma (~50 Hz) frequencies.

(B) Power of gamma oscillations for each of the tetrodes shown in Figure 3A. Bars indicate mean (± SEM) power during detected gamma intervals. Note the gradient of intensity from dorsal/lateral striatum (#1) to ventral/medial striatum (nucleus accumbens; #5), opposite to that of HVS power (Figure 3D).

(C) Coherence of striatal ~8 Hz oscillations to hippocampal theta during task performance. Hippocampal LFP was simultaneously measured from tetrodes placed in dorsal hippocampal CA1 region, pyramidal layer (as in Figure 6A, right). Coherence is a normalized estimate of the strength of coupling between two processes, ranging from 0 (full independence) to 1 (Halliday et al., 1995). Coherence between striatum and hippocampus at theta frequency was strong in ventral/medial striatum and weak in dorsal/lateral striatum.

randomly with respect to the phase of hippocampal theta, as revealed in both spike-triggered averages of LFPs and in phase histograms (Figures 6C and 6D). While theta is largely coherent across hippocampal regions, theta phase varies as a function of depth within CA1 (Buzsáki, 2002). However, by recording consistently from the pyramidal cell layer of dorsal CA1, we were able to compare the theta phases of striatal neurons recorded in different sessions or different animals. The overall population of entrained striatal M units tended to fire on the descending phase of this hippocampal theta (i.e., after the theta peaks but before the theta troughs; Figure 6G). On a number of occasions, we recorded theta-entrained and -not entrained M units simultaneously from the same tetrode (Figure 6E), suggesting that these populations are unlikely to be strictly segregated into separate striatal compartments (Gerfen, 1992; Graybiel and Ragsdale, 1978). However, the distribution of theta-entrained M units was graded, with units recorded from dorsal/lateral striatum generally not entrained (Figures 6E and 6F). The striatum thus shows opposite gradients of neuronal entrainment to distinct ~8 Hz rhythms (high-voltage spindles and hippocampal theta).

Discussion

We have shown that distinct populations of single units can be discriminated in extracellular recordings from unrestrained rats. Fast-spiking, tonically active cells, which are likely GABAergic interneurons, are preferentially found in sensorimotor regions of striatum that also show prominent high-voltage spindle oscillations. Fast-spiking units show bursts of spikes at an earlier HVS phase than presumed projection neurons, whose participation in HVSs is correlated with the local density of fast-spiking units. Within cognitive/limbic parts of striatum, fast-spiking units are few, high-voltage spindles are weak, and presumed projection neurons are instead entrained to the hippocampal theta rhythm.

Classification of Striatal Neurons

While there have been a number of attempts to classify extracellularly recorded striatal neurons (reviewed in Wilson, 1993; Bennett and Wilson, 2003), we have presented a clear difference between two classes of striatal neurons in freely moving rats. F units have much briefer action potentials than M units and are tonically active in awake animals. This distinction was confirmed by examining neuronal firing patterns associated with different behavioral states: F units show a characteristic transition from single spikes to high-frequency bursts during slow-wave sleep. Further, we found that F units fire at an earlier phase of high-voltage spindle oscillations than M units. Taken together, this is strong evidence that F and M units represent distinct subpopulations of striatal neurons.

Even though M units constituted three-quarters of our sample, their extended periods of silence and low average firing rates undoubtedly caused them to be undercounted. We can therefore be confident that M units represent medium-spiny projection neurons, which

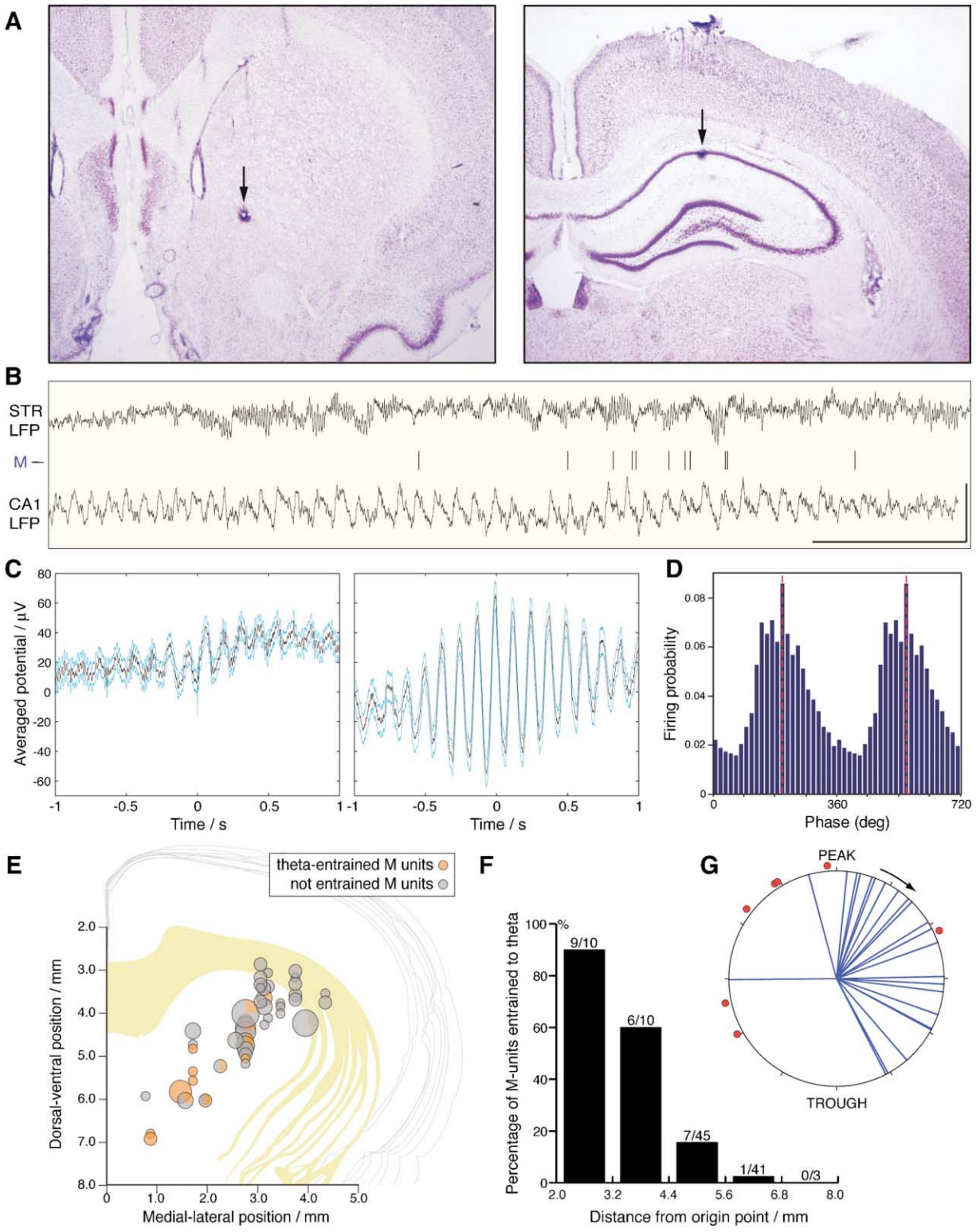

Figure 6. Entrainment of Striatal Single Units to Hippocampal Theta

(A) Simultaneous recording from striatum and hippocampus. Nissl-stained coronal brain sections for a rat in which ten tetrodes targeted ventral/medial striatum (example on left) and four targeted dorsal hippocampal CA1 pyramidal layer (example on right). Arrows indicate small marker lesions created by passing current through tetrodes after recording.

(B) LFPs recorded from the two locations shown in (A), together with spike times for one of the M units recorded from the striatal tetrode, during performance of a radial maze task. Note that theta rhythm is obvious in hippocampus ("CA1 LFP") but less apparent in striatum ("STR LFP"), where higher-frequency (gamma) oscillations predominate. Scale bars, 1 mV, 1 s.

make up the great majority of striatal neurons and are known to have this type of firing pattern in both rats and nonhuman primates (Wilson, 1993). While F units in awake rats were tonically active, they were very unlikely to correspond to the "tonically active neurons" (TANs) that have been studied in nonhuman primates (e.g., Apicella et al., 1991; Blazquez et al., 2002; Kimura et al., 1984). TANs are believed to be cholinergic interneurons, in part because they have very long-duration action potentials (Kimura et al., 1984; Wilson et al., 1990). In intracellular studies comparing distinct classes of rat striatal interneurons, fast-spiking GABAergic interneurons have by far the briefest action potentials and can fire high-frequency bursts (Kawaguchi, 1993; Koos and Tepper, 1999; Plenz and Kitai, 1998). These electrophysiological features reflect the presence of the calcium binding protein parvalbumin (PV) and delayed rectifier potassium channels with fast kinetics, such as Kv3.1 (Jonas et al., 2004; Lenz et al., 1994). PV-staining GABAergic interneurons are heterogeneously distributed within rat striatum, being more common in lateral than medial subregions (Bennett and Bolam, 1994; Cowan et al., 1990; Gerfen et al., 1985; Kita et al., 1990; Kubota and Kawaguchi, 1993), in dorsolateral compared to ventromedial striatum (Gerfen and Wilson, 1996; Lenz et al., 1994; Ramanathan et al., 2002), and in posterior compared to anterior striatum (Kubota and Kawaguchi, 1993). This distribution appears to be unique among well-characterized striatal neuronal populations (Gerfen and Wilson, 1996). Our F units show a graded distribution very similar to that reported for PV-staining GABAergic interneurons, increasing in density rapidly along the medial-lateral axis and somewhat more slowly along the ventral-dorsal and anterior-posterior axes. The combination of distribution, waveform duration, and high-frequency bursts provides strong convergent evidence that our F units correspond to striatal fast-spiking, PV-staining GABAergic interneurons, although it is not possible to prove this with extracellular recordings.

Coordination of Projection Units by GABAergic Interneurons

Individual PV-positive striatal interneurons receive direct, converging glutamatergic synapses from multiple cortical regions (Bennett and Bolam, 1994; Lapper et al., 1992; Ramanathan et al., 2002). They are believed to be more responsive to cortical inputs than the medium-spiny cell population (Parthasarathy and Graybiel, 1997) and to respond to cortical stimulation with brief, high-frequency bursts (Kita, 1993; Richardson et al., 1977). In turn, PV interneurons each provide powerful GABAergic input to a large number of nearby medium-spiny neurons (Koos and Tepper, 1999), via synapses on cell bodies and proximal dendrites (Bennett and Bolam, 1994; Kita et al., 1990). This arrangement allows for strong, widespread, feedforward inhibition (Kita, 1993) that may assist the basal ganglia in selecting one action while suppressing incompatible alternatives (Mink, 1996; Redgrave et al., 1999). A deficit in striatal PV-staining interneurons in the dt^{sz} mutant hamster is associated with paroxysmal dystonia—abnormal cocontractions of opposing muscles (Gernert et al., 2000). Burst firing of fast-spiking striatal interneurons, such as that observed here during HVS, is particularly effective at delaying the firing of medium-spiny neurons (Koos and Tepper, 1999). Our results are consistent with the emerging consensus that PV-containing, fast-spiking interneurons serve to coordinate the timing of spikes in wider neuronal populations, facilitating synchronous, oscillatory activity.

Genesis and Widespread Synchronization of Spindle Oscillations

How do high-voltage spindles get started in striatum? Neural circuits in cortex and thalamus are generally believed to be particularly important in the initiation of all kinds of spindle oscillation, with the thalamic reticular nucleus playing a central pacemaking role (Buzsáki et al., 1988b; Destexhe and Sejnowski, 2001; Steriade et al., 1993). The reticular nucleus has strong projections to thalamic intralaminar nuclei (central-lateral and parafasicular), which in turn project strongly and topographically to the striatum, especially dorsal-lateral striatum (Berendse and Groenewegen, 1990; Herkenham and Pert, 1981; Steriade et al., 1984). Some of these striatal afferents have high axon conduction velocities that potentially contribute to the rapid establishment of striatal spindles (Steriade and Glenn, 1982). Antidromic activation of thalamostriatal projections may be responsible

(C) Spike-triggered averages of the striatal (left) and hippocampal (right) LFPs shown in (B), triggered by all 1336 spikes of the striatal M unit shown in (B) during this session (2101 s duration). Blue lines indicate $\pm 2 \times$ SEM. Theta phase locking of spike times is weakly apparent from the averaged striatal LFP and very clear from the averaged hippocampal LFP. In this example, the spikes of the striatal M unit came shortly after the peaks of hippocampal theta.

(D) Phase histogram for the same M unit relative to the troughs of hippocampal theta (two complete cycles shown for clarity; theta troughs are at 0°/360°/720°). Resultant phase of spikes = −158.9° (indicated by red dashed lines), with entrainment significant at $p < 10^{-57}$. The theta phase precession typical of hippocampal CA1 pyramidal cells was not obviously apparent for striatal M units.

(E) Anatomical distribution of theta-entrained M units (23/109 M units recorded from five rats for which hippocampal CA1 pyramidal layer LFP was recorded during radial maze performance). Unit locations are shown mapped onto stacked coronal atlas sections as in Figures 1C and 2D. Orange circles represent M units that showed a significant ($p < 0.01$) phase relationship to hippocampal theta troughs, while M units that were not significantly theta entrained are shown in gray. The area of the circle is proportional to the number of units simultaneously recorded from that location.

(F) Graded distribution of the set of theta-entrained M units mapped in (E). Graph origin and bins are the same as for Figures 1D and 2E. The numbers over the bars indicate the fraction of M units that were significantly theta entrained.

(G) Phase of theta-entrained striatal units, relative to the troughs of hippocampal theta. Spikes of most striatal M units (blue lines; n = 23) occurred on the descending portion of the hippocampal theta rhythm (mean spike of the entrained M unit population occurred at −126.6°, or ~44 ms before the theta troughs). While most F units were not phase locked to hippocampal theta (7 of 20 tested were significantly entrained at $p < 0.01$), those that were (indicated by red circles) tended to fire at a distinct phase to M units (mean spike of the entrained F unit population occurred at 134.5°, or ~47 ms after the theta troughs).

for the fact that spindles can be evoked in cortical EEG traces by electrical stimulation of the striatum ("caudate spindles"; Buchwald et al., 1961; Buzsáki et al., 1990). However, thalamic regions projecting to striatum appear not to strongly participate in HVSs themselves (Vergnes et al., 1990). Also, while PV-staining interneurons in striatum receive direct innervation from thalamic intralaminar nuclei, this input appears to be rather weak compared to the powerful cortical input to these cells (Ichinohe et al., 2001; Rudkin and Sadikot, 1999). Striatal regions that contain a high-density of PV-interneurons receive input predominantly from lateral cortical regions, including primary motor and somatosensory cortex (Brown et al., 1998; McGeorge and Faull, 1989). High-voltage spindles often appear earlier in somatosensory cortex than other cortical regions (Meeren et al., 2002) and emerge from lower-voltage, transient, less generalized 5–9 Hz oscillations (Pinault et al., 2001) that are common in such lateral cortical regions (J.D.B., unpublished data). Thus, while the rapid entrainment of F units to HVSs may reflect direct inputs from thalamus, it appears more likely to be a response to oscillations within cortical subregions.

The intrinsic properties of the electrically coupled network of striatal GABAergic interneurons may also contribute to their rapid entrainment. These cells have a tendency toward spindle frequency activity (7–15 Hz) even in cortex-striatum cocultures with no thalamus present (Plenz and Aertsen, 1996). Gap junctions may be especially effective for synchronization into such low-frequency oscillations, as they act as low-pass filters (McBain and Fisahn, 2001; Bennett and Zukin, 2004). While we did not perform manipulations of gap junction conductance in this study, burst firing of electrically coupled fast-spiking neurons in thalamic reticular nucleus is highly effective at synchronizing these cells into spindle frequency oscillations in vitro (Landisman et al., 2002; Long et al., 2004).

While the thalamic reticular nucleus is a likely pacemaker for striatal spindles, striatal circuits in turn have projections back to the reticular nucleus, via the globus pallidus (O'Donnell et al., 1997). Through such pathways, basal ganglia circuits may influence the onset and coherence of oscillations in thalamus and cortex (Buzsáki et al., 1990). For example, interference with striatal dopaminergic transmission, either by intrastriatal injections of dopamine D_2 receptor antagonists or lesion of the nigrostriatal pathway, greatly increases the incidence of cortical high-voltage spindles (Buonamici et al., 1986; Buzsáki et al., 1990; Semba and Komisaruk, 1984).

Significance of High-Voltage Spindles

The high-voltage spindle oscillations examined here occur in unpredictable episodes during awake immobility (unlike "sleep spindles," which are higher-frequency, less generalized oscillations seen during sleep). They are often associated with a fine tremor of the whiskers and face (Fanselow et al., 2001; Semba and Komisaruk, 1984), though not always (Buzsáki et al., 1988b; Hartmann and Bower, 1998). HVSs are seen more often in aged than young animals (Buzsáki et al., 1988a), more often in some rat and mouse strains than others (Buzsáki et al., 1990), and even within strains show great individual variation in how often they appear. The same oscillations have been referred to under a bewildering variety of names, including high-voltage spindles (Buzsáki et al., 1988b), spike wave discharges (e.g., Meeren et al., 2002), alpha oscillation (Semba et al., 1980), mu rhythm (MacKay, 1997), sensorimotor rhythm (Nicolelis et al., 1995) or simply "7–12 Hz oscillations" (Castro-Alamancos and Connors, 1996). In part, this reflects a long-standing difference of opinion about their functional significance (see e.g., Ryan, 1984). For some investigators, these oscillations have represented a distinct, functional mode of thalamocortical circuits (Castro-Alamancos and Connors, 1996) that is optimized for detecting weak or novel forms of whisker stimulation (Nicolelis et al., 1995; Nicolelis and Fanselow, 2002). For others, these oscillations are more akin to a seizure, and they are widely used as a model of generalized absence epilepsy (for discussion of this point, see Buzsáki et al., 1990). Recently, however, it has been shown that during HVSs rats are no less and no more responsive to fine tactile stimuli than outside of HVSs (Wiest and Nicolelis, 2003). As rats are not perceptually "absent," the ~8 Hz HVSs clearly do not have the same impact on neural processing as the ~3 Hz spike-and-wave oscillations characteristic of human absence epilepsy, even if the two types of oscillation use overlapping neural mechanisms.

We note that high-voltage spindles generally occur when there is no strong motivation to act—for example, once the local environment has been thoroughly explored. It has been suggested that the role of the basal ganglia in action selection and initiation is achieved through their ability to switch local regions of cortex from an "idling state" characterized by spindle/alpha frequency rhythms to an active state characterized by gamma band synchrony (Brown and Marsden, 1998). High-voltage spindles may be a resonant mode of thalamocortical circuits that is facilitated and generalized when basal ganglia networks are not selecting any particular action—either because no course of action has a strong motivational pull on behavior or because dopamine blockade reduces the probability that any action will be selected.

Cellular Entrainment to Ventral Striatal Rhythms

When our rats were actively running through a maze task, oscillatory activity was less prominent in sensorimotor striatum, and distinct theta, beta, and gamma oscillations were present in cognitive/limbic striatum. The absence of a laminar organization within basal ganglia nuclei can present difficulties in interpretation of local field potentials, as it is impossible to separate sources and sinks of current arising from cell bodies versus dendrites. Intracellular studies in anesthetized rats have shown a close relationship between negative shifts in ventral striatal LFPs and membrane depolarization of spiny neuron ensembles (Goto and O'Donnell, 2001a; Leung and Yim, 1993), and subthreshold beta/gamma frequency oscillations have been reported in the membrane potential of spiny neurons upon cortical desynchronization (Kasanetz et al., 2002). However, it is not currently practical to perform intracellular recordings in freely moving animals. Entrainment of single units to LFP oscillations is therefore one important form

of evidence that such oscillations truly reflect local processes rather than volume conduction from other structures. Beta and gamma entrainment of our M units was, in the great majority of cases, not obvious from spike-triggered averages and phase histograms. Entrainment to beta oscillations has been recently reported in monkey striatum (Courtemanche et al., 2003), though this appeared to be very weak. Unit participation in striatal beta and gamma rhythms may be more fleeting and more dependent on specific types of behavior than the robust entrainment to theta and HVSs reported here—we are currently investigating this possibility.

Our observation of a close relationship between ventral/medial striatum and hippocampal activity in behaving rats is consistent with prior work in anesthetized animals. In this condition, striatal spiny neurons show bistability of their membrane potential, switching between the resting "down" state (−80 mV) and the "up" state (−60 mV), from which action potentials can be fired. Burst activity of hippocampal CA1 cells, during sleep "ripples," is associated with transitions to the up state in striatal spiny neurons (Goto and O'Donnell, 2001b). Inactivation or transection of the fornix, which carries hippocampal inputs to ventral/medial striatum, abolishes these transitions (O'Donnell and Grace, 1995) and the corresponding striatal LFP shifts (Goto and O'Donnell, 2001a). While it remains to be directly demonstrated that up/down bistability is actually present in awake behaving animals—there is evidence that during cortical desynchronization neurons are near-continuously in the more depolarized state (Kasanetz et al., 2002; Steriade et al., 2001)—it has been argued that theta frequency up/down alternation may be a key feature of neuronal activity that serves to "gate" information processing in ventral/medial striatum (Murer et al., 2002).

While we recorded theta from dorsal CA1, the striatum receives input from multiple hippocampal regions, particularly from subiculum (Groenewegen et al., 1987; Kelley and Domesick, 1982). Even beyond the hippocampus proper, theta entrainment of neuronal populations is found in multiple regions that converge upon ventral/medial striatum, including amygdala (Pare and Gaudreau, 1996), deep entorhinal cortex (Sorensen, 1985), and medial frontal cortex (J.D.B. unpublished data). As the interaction between these inputs depends upon their relative timing (Goto and O'Donnell, 2002), theta and theta phase differences between inputs may be an important mechanism for the functional role of ventral/medial striatum as a "limbic-motor interface" (Mogenson et al., 1980) in goal-directed behavior.

Experimental Procedures

Electrophysiology

All animals were housed on a 12 hr:12 hr light/dark cycle, with experiments performed during the light phase. Data presented here were obtained from nine adult male Long-Evans rats (>300 g), each implanted with one of two chronic electrode configurations. For each of six rats, 14 individually drivable tetrodes (four 12.5 μm nichrome wires twisted together; Wilson and McNaughton, 1994) were directed toward various striatal locations (e.g., Figure 3A) and toward dorsal hippocampus (3.6 mm posterior and 2.2 mm lateral to bregma). For each of three other rats, bundles of stereotrodes (twisted pairs of 25 μm nichrome wires) were implanted into six distinct striatal subregions (e.g., Figure 4A). In both configurations, skull screws were placed in contact with multiple cortical regions to record EEG signals. Additional skull screws served as ground (posterior lateral skull ridge) or as a reference for LFP/EEG signals (approximately 1 mm posterior to lambda, except as noted). Data acquisition was performed using a 96 channel system built around custom amplifiers (Boston University Electronics Design Facility) and the real-time Linux program Spike by Loren Frank. This system also acquired synchronized digital video images. EEG and LFP signals were filtered at 0.1–600 Hz and digitized continuously at 1024 Hz or 1500 Hz (similar or identical striatal oscillations were observed at both sampling rates). Extracellular spikes were filtered at 600 Hz to 6 kHz and digitized at 30 kHz. Following implantation, animals were recorded for several weeks to several months during rest sessions (30–60 min) and during performance of a radial maze task; in some animals, striatal electrodes were lowered at ~100 μm intervals after recording each day in order to sample from a wide range of depths. At the end of experiments, current (50 μA, 10 s) was passed through electrode tips to create small marker lesions, and rats were perfused with potassium ferrocyanide to facilitate localization. Locations within striatum were mapped onto coordinates in a reference brain atlas (Swanson, 1992) using MorphAge software. In this study, we did not assess hemispheric asymmetries; for power and unit distribution analyses, left and right striata were merged.

Data Analysis

EEG and LFP signals were analyzed using custom routines written in MATLAB (Mathworks Inc.). To identify intervals of high power in spindle (7–14 Hz), ripple (120–200 Hz), or gamma (35–100 Hz) frequency ranges, LFP signals were first bandpass filtered using digital filters constructed via the Parks-McClellan optimal equiripple FIR design. Peaks and troughs in the filtered signal were found using a peak detection algorithm, and those that exceeded a specific voltage threshold J and were separated by less than a time parameter Δ were grouped together (adapted from Siapas and Wilson, 1998); groups spanning more than a minimum interval length were designated as intervals. To choose a voltage threshold, we used an iterative algorithm that found a threshold Ω that produced one single interval that satisfied all criteria; J was generally set to $0.35 \times \Omega$. For hippocampal theta intervals, an additional criterion of a >4-fold ratio between theta (5–9 Hz) and delta (2–4 Hz) power was applied. Although theta and high-voltage spindles have a similar ~8 Hz base frequency, they were easily distinguished both by the distinctive "spike-and-wave" shape of HVS cycles and by their very different behavioral correlates (immobility versus active movement). Prolonged (>1 min) epochs of slow-wave sleep were manually scored by the joint presence of obvious large-amplitude slow waves (delta frequency, 0.5–3 Hz) in the cortical EEG, ripples in the hippocampal LFP, and the rat's lying down with eyes closed in the video record.

For each HVS interval detected, the HVS onset was defined as the start time of a one-cycle time window, closest to the start of the interval, such that the average 7–14 Hz filtered power within the window was 25% of the average 7–14 Hz filtered HVS power within the interval. Sliding time windows were tested from ten cycles before the start to one cycle before the end of the interval. The duration of a cycle was automatically computed as $1/F_i$, where F_i is the frequency of peak power in the spectrum of the filtered LFP or EEG signal within the interval. To ensure that onset points were detected only for episodes that had a nearly monotonic increase in power around the start of the interval, an onset point was disqualified if the window power exceeded 25% of average interval power within a five-cycle window preceding the onset point.

Power spectral density (PSD) estimates were computed via Welch's method, using nonoverlapping rectangular windows of 512 samples (0.5 s) for FFT calculations in the range 0–128 Hz (0.125 Hz resolution), followed by smoothing with a 3 point moving average.

Neuronal action potentials were manually assigned to unit clusters using Offline Sorter (Plexon Inc.). Units that fired less than 50 spikes during a recording session were excluded. To determine the phase relationship between single cells and spindles, the sharp peaks ("spikes" of spike wave discharges) were detected in the raw striatal LFP using a peak detection algorithm within detected HVS intervals. Each action potential occurring between two successive peaks was assigned a corresponding phase (Klausberger et al., 2003). All HVS

cycles were superimposed to compute a mean phase and its significance for each unit and for each population, using standard circular statistical methods (Durand and Greenwood, 1958; Zar, 1974). Phase relationships between spikes and hippocampal theta were calculated in the same way, except that peaks were detected in the hippocampal dorsal CA1 pyramidal layer LFP, prefiltered at 5–11 Hz.

To estimate the gradients of HVS and gamma power within striatum, we fitted hypersurfaces of the form $S = ax + by + cz + k$ to the power measurements using multiple regression. Here, x, y, and z are the orthogonal anterior-posterior, medial-lateral, and dorsal-ventral brain axes. The direction in which power changed most rapidly was then given by the gradient of S, which is the vector [a b c].

To estimate the gradient of relative F unit density, we first calculated the local density by calculating the proportion of F units in a sphere around each unit. We then calculated a gradient vector in the same way as for HVS and gamma power distributions. A wide range of sphere radii (from 1.4 to 3.9 mm) gave nearly identical results ($r^2 > 0.75$); the best linear fit to the density was obtained with a radius of 2.32 mm.

Acknowledgments

We thank Peter Magill, Anna Grzymała-Busse, Michael Hasselmo, Nancy Kopell, Ana Nathe, Nicholas Sanderson, and John White for comments on earlier versions of the manuscript; and Lotus McDougal for technical assistance. This work was supported by grants from the National Institute on Drug Abuse and the National Institutes of Mental Health to J.D.B.

Received: July 8, 2003
Revised: July 6, 2004
Accepted: August 24, 2004
Published: September 15, 2004

References

Albin, R.L., Young, A.B., and Penney, J.B. (1989). The functional anatomy of basal ganglia disorders. Trends Neurosci. *12*, 366–375.

Alonso, A., and Garcia-Austt, E. (1987). Neuronal sources of theta rhythm in the entorhinal cortex of the rat. II. Phase relations between unit discharges and theta field potentials. Exp. Brain Res. *67*, 502–509.

Apicella, P., Scarnati, E., and Schultz, W. (1991). Tonically discharging neurons of monkey striatum respond to preparatory and rewarding stimuli. Exp. Brain Res. *84*, 672–675.

Bennett, B.D., and Bolam, J.P. (1994). Synaptic input and output of parvalbumin-immunoreactive neurons in the neostriatum of the rat. Neuroscience *62*, 707–719.

Bennett, B.D., and Wilson, C.J. (2003). TANs, PANs and STANs. In The Basal Ganglia VI, A.M. Graybiel, M.R. DeLong, and S.T. Kitai, eds. (New York: Plenum Press).

Bennett, M.V.L., and Zukin, R.S. (2004). Electrical coupling and neuronal synchronization in the mammalian brain. Neuron *41*, 495–511.

Berendse, H.W., and Groenewegen, H.J. (1990). Organization of the thalamostriatal projections in the rat, with special emphasis on the ventral striatum. J. Comp. Neurol. *299*, 187–228.

Bergman, H., Feingold, A., Nini, A., Raz, A., Slovin, H., Abeles, M., and Vaadia, E. (1998). Physiological aspects of information processing in the basal ganglia of normal and parkinsonian primates. Trends Neurosci. *21*, 32–38.

Berke, J.D., and Hyman, S.E. (2000). Addiction, dopamine, and the molecular mechanisms of memory. Neuron *25*, 515–532.

Blazquez, P.M., Fujii, N., Kojima, J., and Graybiel, A.M. (2002). A network representation of response probability in the striatum. Neuron *33*, 973–982.

Brown, P., and Marsden, C.D. (1998). What do the basal ganglia do? Lancet *351*, 1801–1804.

Brown, L.L., Smith, D.M., and Goldbloom, L.M. (1998). Organizing principles of cortical integration in the rat neostriatum: corticostriate map of the body surface is an ordered lattice of curved laminae and radial points. J. Comp. Neurol. *392*, 468–488.

Buchwald, N.A., Wyers, E.J., Okuma, T., and Heuser, G. (1961). The "caudate-spindle". I. Electrophysiological properties. Electroencephalogr. Clin. Neurophysiol. *13*, 509–518.

Buonamici, M., Maj, R., Pagani, F., Rossi, A.C., and Khazan, N. (1986). Tremor at rest episodes in unilaterally 6-OHDA-induced substantia nigra lesioned rats: EEG-EMG and behavior. Neuropharmacology *25*, 323–325.

Buzsáki, G. (2002). Theta oscillations in the hippocampus. Neuron *33*, 325–340.

Buzsáki, G., Bickford, R.G., Armstrong, D.M., Ponomareff, G., Chen, K.S., Ruiz, R., Thal, L.J., and Gage, F.H. (1988a). Electric activity in the neocortex of freely moving young and aged rats. Neuroscience *26*, 735–744.

Buzsáki, G., Bickford, R.G., Ponomareff, G., Thal, L.J., Mandel, R., and Gage, F.H. (1988b). Nucleus basalis and thalamic control of neocortical activity in the freely moving rat. J. Neurosci. *8*, 4007–4026.

Buzsáki, G., Smith, A., Berger, S., Fisher, L.J., and Gage, F.H. (1990). Petit mal epilepsy and parkinsonian tremor: hypothesis of a common pacemaker. Neuroscience *36*, 1–14.

Castro-Alamancos, M.A., and Connors, B.W. (1996). Short-term plasticity of a thalamocortical pathway dynamically modulated by behavioral state. Science *272*, 274–277.

Cobb, S.R., Buhl, E.H., Halasy, K., Paulsen, O., and Somogyi, P. (1995). Synchronization of neuronal activity in hippocampus by individual GABAergic interneurons. Nature *378*, 75–78.

Courtemanche, R., Fujii, N., and Graybiel, A.M. (2003). Synchronous, focally modulated beta-band oscillations characterize local field potential activity in the striatum of awake behaving monkeys. J. Neurosci. *23*, 11741–11752.

Cowan, R.L., Wilson, C.J., Emson, P.C., and Heizmann, C.W. (1990). Parvalbumin-containing GABAergic interneurons in the rat neostriatum. J. Comp. Neurol. *302*, 197–205.

Cummings, J.L. (1993). Frontal-subcortical circuits and human behavior. Arch. Neurol. *50*, 873–880.

Destexhe, A., and Sejnowski, T. (2001). Thalamocortical Assemblies (Oxford, UK: Oxford University Press).

Durand, D., and Greenwood, J.A. (1958). Modifications of the Rayleigh test for uniformity in analysis of two-dimensional orientation data. J. Geol. *66*, 229–238.

Eichenbaum, H., and Cohen, N.J. (2001). From Conditioning to Conscious Recollection: Memory Systems of the Brain (New York: Oxford University Press).

Fanselow, E.E., Sameshima, K., Baccala, L.A., and Nicolelis, M.A. (2001). Thalamic bursting in rats during different awake behavioral states. Proc. Natl. Acad. Sci. USA *98*, 15330–15335.

Galarreta, M., and Hestrin, S. (2001). Electrical synapses between GABA-releasing interneurons. Nat. Rev. Neurosci. *2*, 425–433.

Gerfen, C.R. (1992). The neostriatal mosaic: multiple levels of compartmental organization in the basal ganglia. Annu. Rev. Neurosci. *15*, 285–320.

Gerfen, C.R., and Wilson, C.J. (1996). The basal ganglia. In Handbook of Chemical Neuroanatomy, Volume 12: Integrated Systems of the CNS, Part IIII, L.W. Swanson, A. Bjorklund, and T. Hokfelt, eds. (London: Elsevier), pp. 371–468.

Gerfen, C.R., Baimbridge, K.G., and Miller, J.J. (1985). The neostriatal mosaic: compartmental distribution of calcium-binding protein and parvalbumin in the basal ganglia of the rat and monkey. Proc. Natl. Acad. Sci. USA *82*, 8780–8784.

Gernert, M., Hamann, M., Bennay, M., Loscher, W., and Richter, A. (2000). Deficit of striatal parvalbumin-reactive GABAergic interneurons and decreased basal ganglia output in a genetic rodent model of idiopathic paroxysmal dystonia. J. Neurosci. *20*, 7052–7058.

Gibson, J.R., Beierlein, M., and Connors, B.W. (1999). Two networks of electrically coupled inhibitory neurons in neocortex. Nature *402*, 75–79.

Goto, Y., and O'Donnell, P. (2001a). Network synchrony in the nucleus accumbens in vivo. J. Neurosci. *21*, 4498–4504.

Goto, Y., and O'Donnell, P. (2001b). Synchronous activity in the hippocampus and nucleus accumbens in vivo. J. Neurosci. *21*, RC131.

Goto, Y., and O'Donnell, P. (2002). Timing-dependent limbic-motor synaptic integration in the nucleus accumbens. Proc. Natl. Acad. Sci. USA *99*, 13189–13193.

Graybiel, A.M., and Ragsdale, C.W., Jr. (1978). Histochemically distinct compartments in the striatum of human, monkeys, and cat demonstrated by acetylthiocholinesterase staining. Proc. Natl. Acad. Sci. USA *75*, 5723–5726.

Graybiel, A.M., Aosaki, T., Flaherty, A.W., and Kimura, M. (1994). The basal ganglia and adaptive motor control. Science *265*, 1826–1831.

Groenewegen, H.J., Vermeulen-Van der Zee, E., te Kortschot, A., and Witter, M.P. (1987). Organization of the projections from the subiculum to the ventral striatum in the rat. A study using anterograde transport of Phaseolus vulgaris leucoagglutinin. Neuroscience *23*, 103–120.

Halliday, D.M., Rosenberg, J.R., Amjad, A.M., Breeze, P., Conway, B.A., and Farmer, S.F. (1995). A framework for the analysis of mixed time series/point process data—theory and application to the study of physiological tremor, single motor unit discharges and electromyograms. Prog. Biophys. Mol. Biol. *64*, 237–278.

Hartmann, M.J., and Bower, J.M. (1998). Oscillatory activity in the cerebellar hemispheres of unrestrained rats. J. Neurophysiol. *80*, 1598–1604.

Herkenham, M., and Pert, C.B. (1981). Mosaic distribution of opiate receptors, parafascicular projections and acetylcholinesterase in rat striatum. Nature *291*, 415–418.

Hurtado, J.M., Gray, C.M., Tamas, L.B., and Sigvardt, K.A. (1999). Dynamics of tremor-related oscillations in the human globus pallidus: a single case study. Proc. Natl. Acad. Sci. USA *96*, 1674–1679.

Ichinohe, N., Iwatsuki, H., and Shoumura, K. (2001). Intrastriatal targets of projection fibers from the central lateral nucleus of the rat thalamus. Neurosci. Lett. *302*, 105–108.

Jonas, P., Bischofberger, J., Fricker, D., and Miles, R. (2004). Interneuron diversity series: Fast in, fast out—temporal and spatial signal processing in hippocampal interneurons. Trends Neurosci. *27*, 30–40.

Kandel, A., and Buzsáki, G. (1997). Cellular-synaptic generation of sleep spindles, spike-and-wave discharges, and evoked thalamocortical responses in the neocortex of the rat. J. Neurosci. *17*, 6783–6797.

Kasanetz, F., Riquelme, L.A., and Murer, M.G. (2002). Disruption of the two-state membrane potential of striatal neurones during cortical desynchronisation in anaesthetised rats. J. Physiol. *543*, 577–589.

Kawaguchi, Y. (1993). Physiological, morphological, and histochemical characterization of three classes of interneurons in rat neostriatum. J. Neurosci. *13*, 4908–4923.

Kelley, A.E., and Domesick, V.B. (1982). The distribution of the projection from the hippocampal formation to the nucleus accumbens in the rat: an anterograde- and retrograde-horseradish peroxidase study. Neuroscience *7*, 2321–2335.

Kimura, M., Rajkowski, J., and Evarts, E. (1984). Tonically discharging putamen neurons exhibit set-dependent responses. Proc. Natl. Acad. Sci. USA *81*, 4998–5001.

Kita, H. (1993). GABAergic circuits of the striatum. Prog. Brain Res. *99*, 51–72.

Kita, H., Kosaka, T., and Heizmann, C.W. (1990). Parvalbumin-immunoreactive neurons in the rat neostriatum: a light and electron microscopic study. Brain Res. *536*, 1–15.

Klausberger, T., Magill, P.J., Marton, L.F., Roberts, J.D., Cobden, P.M., Buzsaki, G., and Somogyi, P. (2003). Brain-state- and cell-type-specific firing of hippocampal interneurons in vivo. Nature *421*, 844–848.

Koos, T., and Tepper, J.M. (1999). Inhibitory control of neostriatal projection neurons by GABAergic interneurons. Nat. Neurosci. *2*, 467–472.

Kubota, Y., and Kawaguchi, Y. (1993). Spatial distributions of chemically identified intrinsic neurons in relation to patch and matrix compartments of rat neostriatum. J. Comp. Neurol. *332*, 499–513.

Kubota, Y., Mikawa, S., and Kawaguchi, Y. (1993). Neostriatal GABAergic interneurones contain NOS, calretinin or parvalbumin. Neuroreport *5*, 205–208.

Landisman, C.E., Long, M.A., Beierlein, M., Deans, M.R., Paul, D.L., and Connors, B.W. (2002). Electrical synapses in the thalamic reticular nucleus. J. Neurosci. *22*, 1002–1009.

Lapper, S.R., Smith, Y., Sadikot, A.F., Parent, A., and Bolam, J.P. (1992). Cortical input to parvalbumin-immunoreactive neurones in the putamen of the squirrel monkey. Brain Res. *580*, 215–224.

Lenz, S., Perney, T.M., Qin, Y., Robbins, E., and Chesselet, M.F. (1994). GABA-ergic interneurons of the striatum express the Shaw-like potassium channel Kv3.1. Synapse *18*, 55–66.

Leung, L.S., and Yim, C.Y. (1993). Rhythmic delta-frequency activities in the nucleus accumbens of anesthetized and freely moving rats. Can. J. Physiol. Pharmacol. *71*, 311–320.

Long, M.A., Landisman, C.E., and Connors, B.W. (2004). Small clusters of electrically coupled neurons generate synchronous rhythms in the thalamic reticular nucleus. J. Neurosci. *24*, 341–349.

MacKay, W.A. (1997). Synchronized neuronal oscillations and their role in motor processes. Trends Cogn. Sci. *1*, 176–183.

Magill, P.J., Bolam, J.P., and Bevan, M.D. (2000). Relationship of activity in the subthalamic nucleus-globus pallidus network to cortical electroencephalogram. J. Neurosci. *20*, 820–833.

Mahon, S., Deniau, J.M., and Charpier, S. (2001). Relationship between EEG potentials and intracellular activity of striatal and corticostriatal neurons: an in vivo study under different anesthetics. Cereb. Cortex *11*, 360–373.

McBain, C.J., and Fisahn, A. (2001). Interneurons unbound. Nat. Rev. Neurosci. *2*, 11–23.

McGeorge, A.J., and Faull, R.L. (1989). The organization of the projection from the cerebral cortex to the striatum in the rat. Neuroscience *29*, 503–537.

Meeren, H.K., Pijn, J.P., Van Luijtelaar, E.L., Coenen, A.M., and Lopes da Silva, F.H. (2002). Cortical focus drives widespread corticothalamic networks during spontaneous absence seizures in rats. J. Neurosci. *22*, 1480–1495.

Mink, J.W. (1996). The basal ganglia: focused selection and inhibition of competing motor programs. Prog. Neurobiol. *50*, 381–425.

Mogenson, G.J., Jones, D.L., and Yim, C.Y. (1980). From motivation to action: functional interface between the limbic system and the motor system. Prog. Neurobiol. *14*, 69–97.

Murer, M.G., Tseng, K.Y., Kasanetz, F., Belluscio, M., and Riquelme, L.A. (2002). Brain oscillations, medium spiny neurons, and dopamine. Cell. Mol. Neurobiol. *22*, 611–632.

Nicolelis, M.A., and Fanselow, E.E. (2002). Thalamocortical [correction of Thalamcortical] optimization of tactile processing according to behavioral state. Nat. Neurosci. *5*, 517–523.

Nicolelis, M.A., Baccala, L.A., Lin, R.C., and Chapin, J.K. (1995). Sensorimotor encoding by synchronous neural ensemble activity at multiple levels of the somatosensory system. Science *268*, 1353–1358.

O'Donnell, P., and Grace, A.A. (1995). Synaptic interactions among excitatory afferents to nucleus accumbens neurons: hippocampal gating of prefrontal cortical input. J. Neurosci. *15*, 3622–3639.

O'Donnell, P., Lavin, A., Enquist, L.W., Grace, A.A., and Card, J.P. (1997). Interconnected parallel circuits between rat nucleus accumbens and thalamus revealed by retrograde transynaptic transport of pseudorabies virus. J. Neurosci. *17*, 2143–2167.

Paré, D., and Gaudreau, H. (1996). Projection cells and interneurons of the lateral and basolateral amygdala: distinct firing patterns and differential relation to theta and delta rhythms in conscious cats. J. Neurosci. *16*, 3334–3350.

Parthasarathy, H.B., and Graybiel, A.M. (1997). Cortically driven immediate-early gene expression reflects modular influence of sensorimotor cortex on identified striatal neurons in the squirrel monkey. J. Neurosci. *17*, 2477–2491.

Pinault, D., Vergnes, M., and Marescaux, C. (2001). Medium-voltage 5-9-Hz oscillations give rise to spike-and-wave discharges in a genetic model of absence epilepsy: in vivo dual extracellular recording of thalamic relay and reticular neurons. Neuroscience *105*, 181–201.

Plenz, D., and Aertsen, A. (1996). Neural dynamics in cortex-striatum co-cultures—II. Spatiotemporal characteristics of neuronal activity. Neuroscience *70*, 893–924.

Plenz, D., and Kitai, S.T. (1998). Up and down states in striatal medium spiny neurons simultaneously recorded with spontaneous activity in fast-spiking interneurons studied in cortex-striatum-substantia nigra organotypic cultures. J. Neurosci. *18*, 266–283.

Plenz, D., and Kitai, S.T. (1999). A basal ganglia pacemaker formed by the subthalamic nucleus and external globus pallidus. Nature *400*, 677–682.

Ramanathan, S., Hanley, J.J., Deniau, J.M., and Bolam, J.P. (2002). Synaptic convergence of motor and somatosensory cortical afferents onto GABAergic interneurons in the rat striatum. J. Neurosci. *22*, 8158–8169.

Redgrave, P., Prescott, T.J., and Gurney, K. (1999). The basal ganglia: a vertebrate solution to the selection problem? Neuroscience *89*, 1009–1023.

Richardson, T.L., Miller, J.J., and McLennan, H. (1977). Mechanisms of excitation and inhibition in the nigrostriatal system. Brain Res. *127*, 219–234.

Rudkin, T.M., and Sadikot, A.F. (1999). Thalamic input to parvalbumin-immunoreactive GABAergic interneurons: organization in normal striatum and effect of neonatal decortication. Neuroscience *88*, 1165–1175.

Ryan, L.J. (1984). Characterization of cortical spindles in DBA/2 and C57BL/6 inbred mice. Brain Res. Bull. *13*, 549–558.

Semba, K., and Komisaruk, B.R. (1984). Neural substrates of two different rhythmical vibrissal movements in the rat. Neuroscience *12*, 761–774.

Semba, K., Szechtman, H., and Komisaruk, B.R. (1980). Synchrony among rhythmical facial tremor, neocortical 'alpha' waves, and thalamic non-sensory neuronal bursts in intact awake rats. Brain Res. *195*, 281–298.

Shaw, F.Z. (2004). Is spontaneous high-voltage rhythmic spike discharge in Long Evans rats an absence-like seizure activity? J. Neurophysiol. *91*, 63–77.

Siapas, A.G., and Wilson, M.A. (1998). Coordinated interactions between hippocampal ripples and cortical spindles during slow-wave sleep. Neuron *21*, 1123–1128.

Sorensen, K.E. (1985). Projections of the entorhinal area to the striatum, nucleus accumbens, and cerebral cortex in the guinea pig. J. Comp. Neurol. *238*, 308–322.

Steriade, M., and Glenn, L.L. (1982). Neocortical and caudate projections of intralaminar thalamic neurons and their synaptic excitation from midbrain reticular core. J. Neurophysiol. *48*, 352–371.

Steriade, M., Parent, A., and Hada, J. (1984). Thalamic projections of nucleus reticularis thalami of cat: a study using retrograde transport of horseradish peroxidase and fluorescent tracers. J. Comp. Neurol. *229*, 531–547.

Steriade, M., McCormick, D.A., and Sejnowski, T.J. (1993). Thalamocortical oscillations in the sleeping and aroused brain. Science *262*, 679–685.

Steriade, M., Timofeev, I., and Grenier, F. (2001). Natural waking and sleep states: a view from inside neocortical neurons. J. Neurophysiol. *85*, 1969–1985.

Swanson, L.W. (1992). Brain Maps: Structure of the Rat Brain (Amsterdam: Elsevier).

Vergnes, M., Marescaux, C., and Depaulis, A. (1990). Mapping of spontaneous spike and wave discharges in Wistar rats with genetic generalized non-convulsive epilepsy. Brain Res. *523*, 87–91.

White, N.M. (1997). Mnemonic functions of the basal ganglia. Curr. Opin. Neurobiol. *7*, 164–169.

Wiest, M.C., and Nicolelis, M.A. (2003). Behavioral detection of tactile stimuli during 7–12 Hz cortical oscillations in awake rats. Nat. Neurosci. *6*, 913–914.

Wilson, C.J. (1993). The generation of natural firing patterns in neostriatal neurons. Prog. Brain Res. *99*, 277–297.

Wilson, M.A., and McNaughton, B.L. (1994). Reactivation of hippocampal ensemble memories during sleep. Science *265*, 676–679.

Wilson, C.J., Chang, H.T., and Kitai, S.T. (1990). Firing patterns and synaptic potentials of identified giant aspiny interneurons in the rat neostriatum. J. Neurosci. *10*, 508–519.

Zar, J.H. (1974). Biostatistical Analysis (New Jersey: Prentice-Hall).